ACS APPLIED MATERIALS & INTERFACES

www.acsami.org

Research Article

Thermoelectric Penta-Silicene with a High Room-Temperature Figure of Merit

Zhibin Gao* and Jian-Sheng Wang

Cite This: *ACS Appl. Mater. Interfaces* 2020, 12, 14298−14307

Read Online

ACCESS | Metrics & More | Article Recommendations | Supporting Information

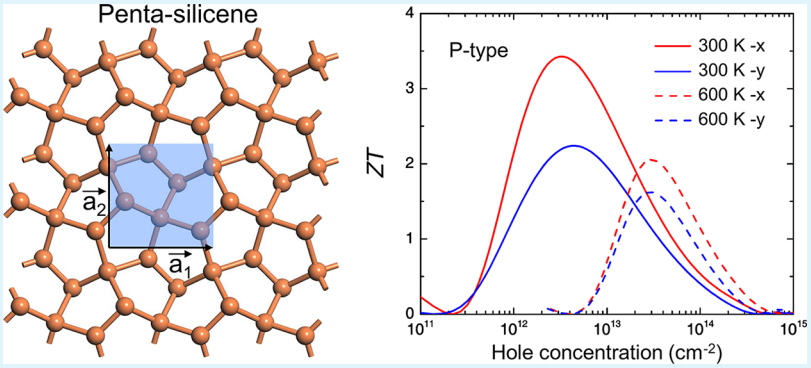

ABSTRACT: Silicon is one of the most frequently used chemical elements of the periodic table in nanotechnology (Goodilin et al., *ACS Nano* **2019**, *13*, 10879−10886). Two-dimensional silicene, a silicon analogue of graphene, has been readily obtained to make field-effect transistors since 2015 (Tao et al., *Nat. Nanotechnol.* **2015**, *10*, 227; Tsai et al., *Nat. Commun.* **2013**, *4*, 1500). Recently, as new members of the silicene family, penta-silicene and its nanoribbon have been experimentally grown on a Ag(110) surface with exotic electronic properties (Cerdá et al., *Nat. Commun.* **2016**, *7*, 13076; Sheng et al., *Nano Lett.* **2018**, *18*, 2937−2942). However, the thermoelectric performance of penta-silicene has not been so far studied, which would hinder its potential applications of electric generation from waste heat and solid-state Peltier coolers. Based on the Boltzmann transport theory and *ab initio* calculations, we find that penta-silicene shows remarkable room-temperature figures of merit ZT of 3.4 and 3.0 at the reachable hole and electron concentrations, respectively. We attribute this high ZT to the superior "pudding-mold" electronic band structure and ultralow lattice thermal conductivity. The discovery provides new insight into the transport property of pentagonal nanostructures and highlights the potential applications of thermoelectric materials at room temperature.

KEYWORDS: *ab initio calculations, penta-silicene, "pudding-mold" electronic structure, figure of merit, thermoelectric property*

INTRODUCTION

The thermoelectric effect directly converts waste heat to electrical energy. Its efficiency is defined by a dimensionless figure of merit ZT, written as $ZT = S^2\sigma T/(\kappa_e + \kappa_L)$ in which S, σ, κ_e, κ_L are the Seebeck coefficient, electrical conductivity, electronic thermal conductivity, and lattice thermal conductivity, respectively. Since S, σ, and κ_e are closely entangled with each other, it is challenging to increase the numerator and decrease the denominator concurrently, gaining a high ZT. Explicitly, an average ZT larger than 2 would make thermoelectric materials without toxic substances attractive and competitive when compared with other types of energy conversion.[7] Furthermore, taking into account the application in daily life, near-room-temperature thermoelectric materials with high ZT are desirably needed.

A reduced κ_L can improve the thermoelectric efficiency, ZT.[8] One can use resonant bonding[9] and lone electron pairs[10] to reduce κ_L. Besides, the power factor $S^2\sigma$ can be augmented by electronic band engineering[11−13] and the quantum confinement effect.[14] Furthermore, two-dimensional (2D) materials have inherent advantages to moderate the contradiction between S and σ due to the tunable electronic band gap, resulting in a high power factor. This is much simpler than in the case of bulk materials. In the case of 2D materials, one has great potential to break the complicated relationship between S and σ due to the quantum confinement effect. This argument was first given by pioneer Mildred Dresselhaus.[14] She also pointed out that one of the advantages of 2D layered materials is that one can actually engineer the band gap. In 2D, one can

Received: November 19, 2019
Accepted: March 3, 2020
Published: March 3, 2020

https://dx.doi.org/10.1021/acsami.9b21076
ACS Appl. Mater. Interfaces 2020, 12, 14298−14307

simply change the number of layers or apply stress/strain to modify the band gap or even tune the chemical bond to modify the electronic band gap.[14]

In 2014, a theoretical work predicted a new 2D carbon allotrope called penta-graphene with favorable stability[15] whose prototype was first proposed in iron-based materials with exotic magnetic frustration.[16] Afterward, the pentagonal system has attracted much attention, such as unexpected thermal conductivity[17−19] and seamless electrical contacts.[20] Recently, a stable penta-silicene was found by reducing the Coulomb interaction of silicon dimers.[21] They also reported that it has an ultrahigh Curie temperature of 1190 K. However, the thermoelectric performance of penta-silicene is still lacking.

In this study, we explore the thermoelectric property of penta-silicene based on the Boltzmann transport theory and *ab initio* calculations. It has good thermal, dynamical, and mechanical stability compared with many typical 2D materials. We find that penta-silicene has a nearly direct band gap of 0.68 eV at the DFT-HSE06 level. Lattice thermal conductivities of penta-silicene have values of 1.66 and 1.29 W/mK along *x*- and *y*-axes, respectively. At room temperature, penta-silicene shows maximum figures of merit ZT of 3.4 and 3.0 at the reachable hole and electron concentrations. Our work indicates that penta-silicene is a promising thermoelectric material, especially near room temperature.

COMPUTATIONAL METHODS

We perform DFT calculations using the projector-augmented-wave (PAW) method,[22,23] Perdew−Burke−Ernzerhof (PBE),[24] and hybrid exchange-correlation HSE06 functional[25,26] with a default mixing parameter value $\alpha = 0.25$ in the VASP code.[27−29] Plane waves with a 550 eV kinetic cutoff energy are used. The vacuum distance between the neighboring layer is set to be 20 Å removing the nonphysical long-range electrostatic interaction. The ionic Hellmann−Feynman forces in each atom and total energy are converged to 10^{-4} eV/Å and 10^{-8} eV in the structure optimization and band calculation. The Brillouin zone is sampled by uniform 21 × 21 × 1. The electronic transport properties are calculated using the electronic Boltzmann transport theory implemented in BoltzTraP.[30] In the phonon calculation, we used a 5 × 5 × 1 supercell and 2 × 2 × 1 k-point sampling to compute the second- and third-order force constants. To solve the phonon Boltzmann transport equation, we adopted a 101 × 101 × 1 Γ-centered q-grid. We also have tested the convergence of lattice thermal conductivity with respect to the cutoff radius, as shown in the Supporting Information. The linearized phonon Boltzmann transport equation is solved by ShengBTE[31] via a full iteration.

RESULTS

Crystal Structure. The optimized monolayer penta-silicene is shown in Figure 1a,b. There are six atoms in the primitive cell indicated by blue shading. From the top view, penta-silicene is the same as penta-graphene.[15] However, penta-silicene has a little distortion compared with penta-graphene.[21] This is due to the tilting of silicon dimers in the penta-silicene in order to reduce the strong Coulomb repulsion and stabilize the crystal structure. It means that one cannot obtain penta-silicene by simple element substitution. One should break the symmetry by moving one of the atoms in order to further lower the energy and reach a local minimum potential profile. The symmetry becomes $P2_1$ (space group no. 4) from $P42_1m$ (space group no. 113). The optimized lattice constants of penta-silicene and penta-graphene, shown in Table 1, are $|\vec{a}_1| = |\vec{a}_2| = 5.58$ and 3.64 Å, respectively, which are in good agreement with previous results.[15,21] It is

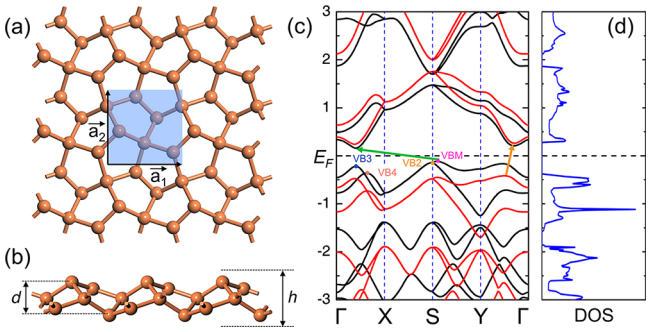

Figure 1. (a, b) Top and side views of the atomic structure of the monolayer penta-silicene in a 3 × 3 supercell. (c) Electronic band structure of penta-silicene using the DFT-PBE (black) and DFT-HSE06 (red) functionals. (d) Electronic density of states (DOS) at the HSE06 level. The indirect fundamental band gaps are marked by the green (PBE) and orange (HSE06) arrows in (c). The Fermi levels are set to zero. The sum of the intrinsic thickness *d* and two van der Waals radii of the outermost atom is defined as the effective thickness *h*. The primitive cell is indicated by blue shading in (a). Four hole pockets in valence bands around the Fermi level are labeled by different colors and numbers (VBM, VB2, VB3, and VB4). VBM denotes the valence band maximum. In the first Brillouin zone, the high symmetry *k* points are: Γ(0 0 0), *X*(1/2 0 0), *S*(1/2 1/2 0), and *Y*(0 1/2 0), respectively.

reasonable due to the augment of atomic size in the same main group IV. Intrinsically, the buckling distance also increases from 1.21 to 2.44 Å from penta-graphene to penta-silicene. The cohesive energy can be calculated by $E_c = (n \times E_{Si} - E_0)/n$ in which E_{si}, E_0, and *n* are the energy of single silicon atom, the energy of the whole system at the equilibrium state, and the number of atoms in the system. The calculated E_c of penta-graphene and penta-silicene are 7.08 and 3.92 eV/atom. Note that, in the experiment, E_c of the experimentally accessible silicene (hexagonal symmetry with two atoms in the primitive cell) and phosphorene are 3.71[32,33] and 3.61 eV/atom,[34,35] respectively. This indicates that the stability of penta-silicene is comparable with hexagonal silicene and black phosphorene, suggesting a robust chemical environment bond to maintain the stability of penta-silicene.

In 3D materials, the elastic tensor is a 6 × 6 tensor with 36 number of tensor elements. By considering the symmetry of the crystal structure, the 6 × 6 tensor can be further simplified according to the specific crystal systems. There are seven crystal systems in solid. The higher the symmetry of the crystal system, the smaller the number of independent tensor elements. For 2D materials, the elastic tensor is a 3 × 3 tensor. To be specific, the mechanical property has a close relationship with phonon modes on the crystal momentum near the center of the Brillouin zone.[36] For penta-silicene, there are three independent elastic components, which are C_{11}, C_{12}, and C_{66}. Note that the value of C_{66} is equal to the shear modulus *G*. The calculated mechanical data of penta-silicene is shown in Table 1. The elastic constants of any stable 2D materials must satisfy $C_{11}C_{22} - C_{12}^2 > 0$ and $C_{66} > 0$. From the table, it can be found that penta-silicene is mechanically stable. Furthermore, the value of C_{12} is −46.88 GPa, indicating a negative in-plane Poisson's ratio that is defined as[37] $\nu_{xy} = \frac{C_{21}}{C_{22}}$ and $\nu_{yx} = \frac{C_{12}}{C_{11}}$. For penta-graphene and penta-silicene, $C_{11} = C_{22}$ and $C_{12} = C_{21}$. C_{11} of penta-silicene is smaller than those of Si-*Cmma* of and Si-*Pmma*,[38] indicating a more flexible mechanical

https://dx.doi.org/10.1021/acsami.9b21076
ACS Appl. Mater. Interfaces 2020, 12, 14298−14307

Table 1. Calculated Physical Properties of Penta-Graphene and Penta-Silicene[a]

materials	$\lvert\vec{a}_1\rvert(\lvert\vec{a}_2\rvert)$ (Å)	d (Å)	h (Å)	E_c (eV/atom)	C_{11} (GPa)	C_{12} (GPa)	G (GPa)	ν
penta-Gr	3.64	1.21	4.61	7.08	584.34	−46.88	328.94	−0.09
penta-Si	5.58	2.44	6.64	3.92	43.13	−23.56	30.31	−0.55

[a] $\lvert\vec{a}_1\rvert(\lvert\vec{a}_2\rvert)$ is the lattice constant. d and h are the intrinsic buckling distance and effective thickness, respectively. E_c is the cohesive energy per atom. C_{ij} is the elastic modulus tensor. G and ν are the shear modulus and Poisson's ratio, respectively.

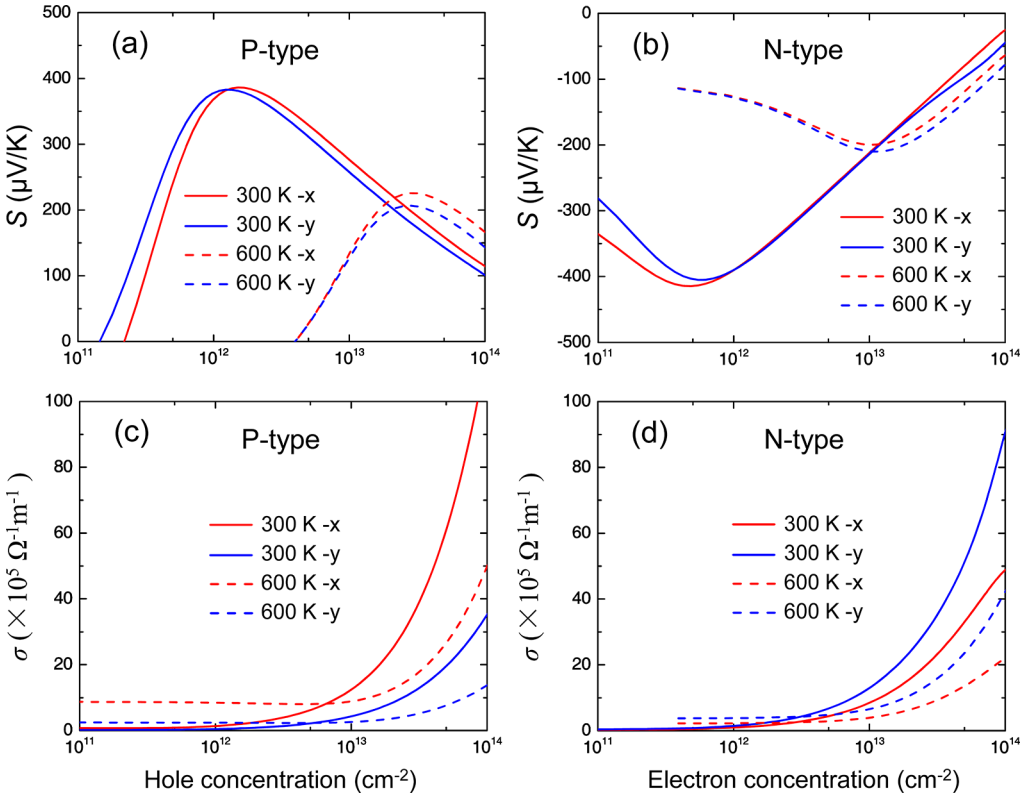

Figure 2. Calculated temperature-dependent electronic transport coefficients. (a, b) Seebeck coefficient S and (c, d) electrical conductivity σ as a function of temperature and carrier concentration (holes and electrons) for x- and y-axis at 300 and 600 K.

properties than other silicon allotropes. The calculated ν of penta-graphene and penta-silicene are −0.09 and −0.55. The value of ν in penta-silicene is 5 times larger than that in penta-graphene. This mechanical property of the negative Poisson's ratio is highly desirable for shock absorption in transistors.[37,39]

Electronic Band Structure. The electronic band structure of penta-silicene is shown in Figure 1c,d. At the PBE level (black), the indirect band gap indicated by the green arrow is 0.28 eV. Since the fundamental band gap is usually underestimated in DFT-PBE calculations, we also calculate it using the HSE06 functional (red). Overall, the entire energy bands are almost unchanged except for the shift up of the conduction bands and the shift down of the valence bands. Interestingly, the HSE06 band shows a nearly direct band gap of 0.68 eV indicated by the orange arrow. This change from the indirect-to-direct band gap would significantly enhance the optical absorbance.[40] Some top valence bands of monolayer penta-silicene around the Fermi level not only are quite close but also are degenerate energetically. The conduction bands around the Fermi level have no similar behavior. We marked the "mountain peaks" of valence bands by different colors and numbers (VBM, VB2, VB3, and VB4). As a matter of fact, these degenerate valence bands will significantly enhance DOS and further Seebeck coefficient[41,42] that directly enters the final figure of merit ZT. Furthermore, since the valence bands are highly degenerate, while conduction bands are nondegenerate, this leads to an asymmetric DOS in Figure 1d. This physical picture is known as "pudding-mold" and desirably required to achieve a large ZT.[11] We will further discuss it in the following.

Electronic Transport Properties. In order to obtain the electronic transport properties, such as Seebeck coefficient S, electrical conductivity σ, and electronic thermal conductivity κ_e, one has to compute the following quantities based on the Boltzmann transport theory, written as a function of the tensor $\mathbf{K}_n$[30,42]

$$\mathbf{K}_n = \frac{2}{(2\pi)^3}\sum_i \int d^3\mathbf{k}\tau_i(\mathbf{k})\mathbf{v}_i(\mathbf{k}) \otimes \mathbf{v}_i(\mathbf{k}) \times [\varepsilon_i(\mathbf{k}) - \mu]^n\left[-\frac{\partial f(\mu, T, \varepsilon_i)}{\partial \varepsilon_i}\right] \quad (1)$$

$$\sigma = e^2\mathbf{K}_0 \quad (2)$$

$$S = \frac{1}{eT}\mathbf{K}_1\mathbf{K}_0^{-1} \quad (3)$$

https://dx.doi.org/10.1021/acsami.9b21076
ACS Appl. Mater. Interfaces 2020, 12, 14298−14307

Table 2. Calculated Effective Masses m_x^*/m_0 and m_y^*/m_0, Deformation Potential Constants E_x and E_y, 2D Elastic Modulus C_x^{2D} and C_y^{2D}, and Carrier Mobilities μ_x^{2D} and μ_y^{2D} Based on eq 7 for x- and y-Axes at 300 K

carrier type	m_x^*/m_0 (G-X)	m_y^*/m_0 (G-Y)	E_x (eV)	E_y (eV)	C_x^{2D} (J m^{-2})	C_y^{2D} (J m^{-2})	μ_x^{2D} (m^2 V^{-1} s^{-1})	μ_y^{2D} (m^2 V^{-1} s^{-1})
electron	0.254	0.430	3.802	2.745	94.753	92.851	0.166	0.185
hole	0.224	1.106	1.546	2.737	94.753	92.851	0.756	0.048

Table 3. Calculated Electronic Relaxation Times τ_e and τ_h, Sound Velocities υ_{TA} and υ_{LA}, Debye Temperatures Θ_{TA} and Θ_{LA} with Definition of $\Theta_D = \hbar\omega/k_B$ Associated with the Maximum Acoustic Phonon Frequency, and Maximum Figure of Merits ZT_e and ZT_h along x- and y-Axes at 300 K[a]

direction	τ_e (ps)	τ_h (ps)	υ_{TA} (km/s)	υ_{LA} (km/s)	Θ_{TA} (K)	Θ_{LA} (K)	ZT_e @300 K	ZT_h @300 K
G-X	0.240	0.964	3.99	4.77	72.32	131.51	2.18	3.43
G-Y	0.453	0.302	4.70	5.54	91.57	105.78	3.04	2.24

[a]The subscripts "e" and "h" indicate electron and hole, respectively.

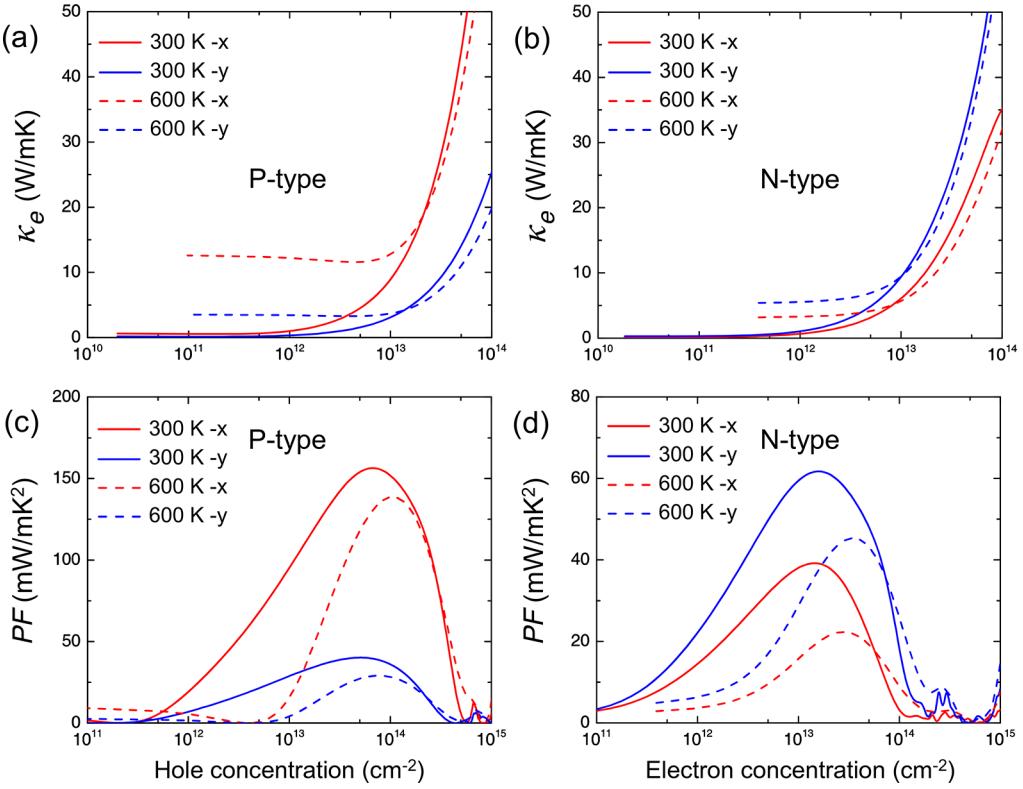

Figure 3. Calculated temperature-dependent electronic transport coefficients of penta-silicene. (a, b) Electronic thermal conductivity (κ_e) and (c, d) power factor $S^2\sigma$ (PF) as a function of temperature and carrier concentration (holes and electrons) along x- and y-axes at 300 and 600 K.

$$\kappa_e = \frac{1}{T}(\mathbf{K}_2 - \mathbf{K}_1{}^2\mathbf{K}_0^{-1}) \tag{4}$$

in which 2 is for the spin degeneracy, $\mathbf{v}_i(\mathbf{k})$ is the electron group velocity of the wave vector $\mathbf{k}$ and band index i. ε_i, μ, and $\tau_i(\mathbf{k})$ are electronic energy, chemical potential, and electronic relaxation time. Alternatively, κ_e can also be calculated through the Wiedemann–Franz law[30,42]

$$\kappa_e = L\sigma T \tag{5}$$

where L is a constant called the Lorenz number with a value of 2.4×10^{-8} W Ω K^{-2}. The calculated κ_e from eqs 4 and 5 are the same for semiconductors, which has been verified by many previous works.[43−45]

Here, we consider two temperatures (300 and 600 K) in the following calculations. The calculated S and σ are shown in Figure 2. For both p-type and n-type doping, S first increases (absolute value) at low carrier concentrations ($n < 10^{12}$ cm^{-2}) and then linearly decreases at high carrier concentrations (10^{12} cm^{-2} < n < 10^{14} cm^{-2}). According to the Mahan–Sofo theory, S for degenerate 2D semiconductors can be written as[8]

$$S_{2D} = \frac{2\pi^3 k_B{}^2 T}{3eh^2 n} m_d^* \tag{6}$$

where h, n, and m_d^* are the Planck constant, carrier concentration, and DOS effective mass around E_F. Since electrons of 2D materials only have freedom in the plane, S_{2D} is quite different from $S_{3D} = \frac{8\pi^2 k_B{}^2 T}{3qh^2} \times \left(\frac{\pi}{3n}\right)^{(2/3)} \times m_d^*$ in bulk materials.[42] Hence, there is a competition relation between n and m_d^*. For high concentrations, our calculated S_{2D} of penta-silicene is inversely proportional to n, which is in good agreement with the Mahan–Sofo theory. For low concen-

https://dx.doi.org/10.1021/acsami.9b21076
ACS Appl. Mater. Interfaces 2020, 12, 14298−14307

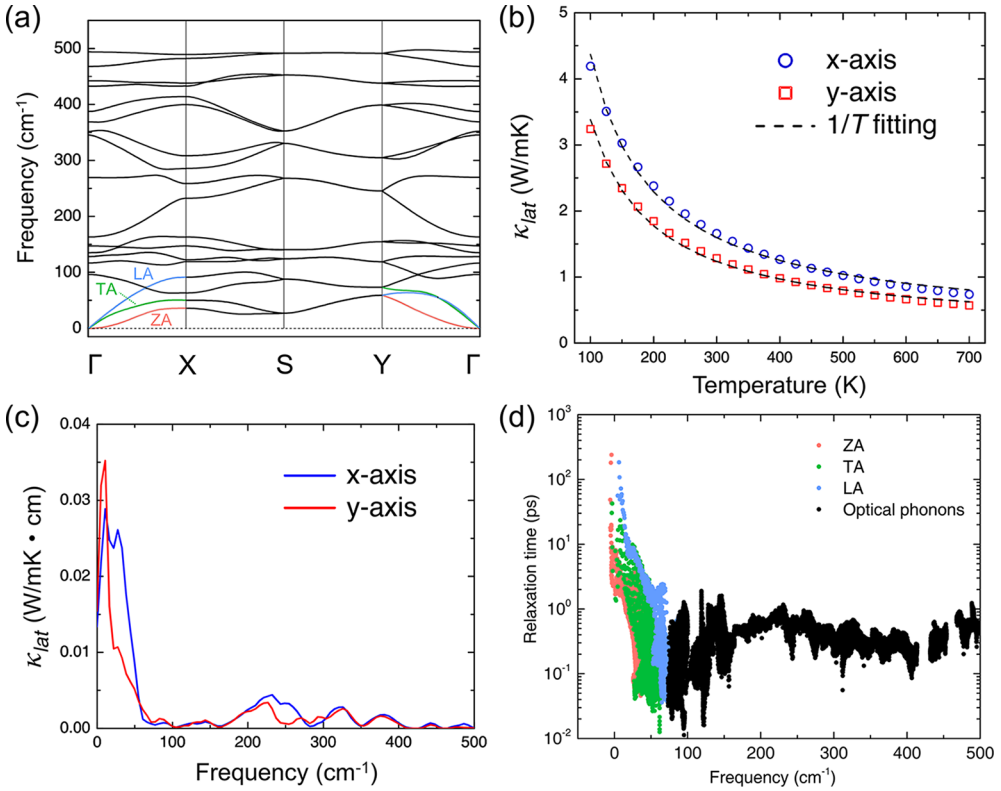

Figure 4. Lattice heat transport properties of penta-silicene. (a) Phonon dispersion, (b) lattice thermal conductivity (κ_L) as a function of temperature, (c) frequency-resolved κ_L along *x*- and *y*-axes at 300 K, and (d) three-phonon relaxation time at room temperature with phonon mode resolution. The acoustic phonon branches (ZA, TA, and LA) are indicated in different colors.

trations, S_{2D} of penta-silicene is induced by the bipolar effect in narrow-band gap semiconductors.[42,46] Interestingly, S_{2D} of penta-silicene at 300 K is generally larger than that at 600 K. The largest S_{2D} of penta-silicene has a value of 400 μ V/K at 10^{12} cm^{-2} carrier concentration for both p- and n-types, which is double of 200 μ V/K of 2D SnSe[47] at the same condition.

Since the output electrical conductivity σ from the conventional Boltzmann transport theory is closely dependent on relaxation time τ, a method to evaluate τ should be applied appropriately. Considering τ in many materials generally have an order of 10−12 ps, some works use a constant number to avoid this dilemma.[48,49] As a matter of fact, there are many factors to impact τ, such as acoustic phonons, nonpolar optical phonons, and ionized impurities. τ in different situations has different expressions.[50] As an accepted rule of thumb, acoustic phonons play the most important role in τ and the acoustic phonon limited carrier mobility μ using the deformation potential (DP) theory of 2D materials can be written as[42]

$$\mu_{2D} = \frac{e\hbar^3 C_{2D}}{k_B T m^* m_d^* E_i^2} \tag{7}$$

in which the parameter can be easily found elsewhere.[42,51] The final relaxation time has a relation with mobility: $\tau = \frac{m^*\mu}{e}$. The calculated data is shown in Table 2. Note that here, we use the single parabolic band model from the original DP theory, which works very well for the nondegenerated electronic band structure. Since penta-silicene has a distortion compared with penta-graphene, the effective mass m^*, and the deformation potential constant E shows a clear anisotropic behavior. Note that in the calculation of E_x and E_y, the energy of hole (electron) must be shifted with respect to the vacuum energy with an expression of $(E^{h,e} - E^{vac}) \propto E^{h,e} \times (\Delta l/l_0)$. The calculated τ of *x*- and *y*-axes, shown in Table 3, are 0.240 and 0.453 ps for electrons, while τ are 0.964 and 0.302 ps for holes, respectively, indicating a large anisotropic transport behavior.

According to eq 7, σ is inversely proportional to the effective mass, contrary to the situation of previous S_{2D}. The calculated σ of penta-silicene is shown in Figure 2c,d. Overall, σ significantly increases as a function of *n*. σ of 300 and 600 K are comparable when $n < 10^{13}$ cm^{-2}. However, σ of 300 K increases faster than σ of 600 K when $n > 10^{13}$ cm^{-2}.

According to eq 5, the electronic thermal conductivity κ_e can be obtained based on σ, as shown in Figure 3a,b. In semiconductors, phonons, especially acoustic phonons, are the main carrier of heat transport. Hence, at low concentrations ($n < 10^{12}$ cm^{-2}), κ_e has a value of around 0.2 W/mK. As *n* increases, penta-silicene is increasingly doped due to the augment of corresponding σ. For a larger *n*, κ_e cannot be neglected since more holes (electrons) are doped and the penta-silicene is more like a good conductor.[19,30]

Generally, *S* decreases and σ increases as a function of carrier concentration. An admirable thermoelectric material needs large *S* and σ simultaneously. Power factor PF ($S^2\sigma$) is a good indicator to describe this joint effect of *S* and σ. The calculated PF is shown in Figure 3c,d. It increases at low concentrations due to the enhancement of *S* and σ. Then, PF decreases after climbing to the top since *S* is suppressed at elevated doping. For p-type, PF along the *x*-axis is larger than that along the *y*-axis. However, n-type is the opposite situation ($PF_y > PF_x$). At 300 K, the maximum PF for p-type doping are 156.40 and

https://dx.doi.org/10.1021/acsami.9b21076
ACS Appl. Mater. Interfaces 2020, 12, 14298−14307

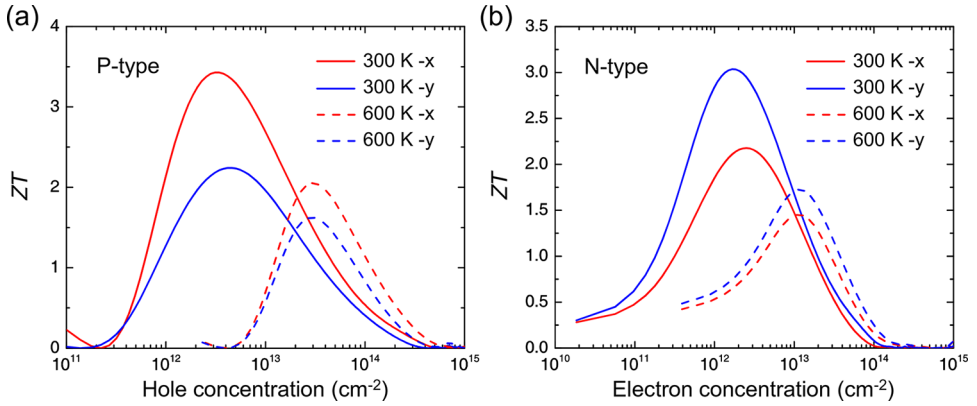

Figure 5. Calculated figure of merit ZT of (a) p-type and (b) n-type penta-silicene as a function of the carrier concentration along *x*- and *y*-axes at 300 and 600 K.

40.23 mW/mK^2 at 5.09 × 10^{13} cm^{-2} concentration along the *x*- and *y*-axes, respectively. Similarly, maximum PF for n-type doping are 61.75 and 39.22 mW/mK^2 at 1.55 × 10^{13} cm^{-2} concentration along both axes at the same temperature. Such PF values are quite larger than those of 2D tellurium (57.3 mW/mK^2)[42] and 2D SnSe (57.3 mW/mK^2).[47]

A good thermoelectric material should satisfy that the distribution of electronic energy carriers at the Fermi level is as narrow as possible, as well as high carrier velocity according to the Mahan's guideline.[52] Subsequently, researchers find an effective approach to enhance the Seebeck coefficient *S* and electrical conductivity σ simultaneously, where the electronic bands around E_F contain both flat and dispersive bands in the dependent momentum space. It is known as a "pudding-mold" band structure.[53,54] Flat bands increase the DOS and dispersive bands induce high carrier velocities. It has been used to explain many prominent thermoelectric performances, such as Na_xCoO_2,[53] SnSe,[55] $PbTe_{1-x}Se_x$,[12] and tellurium.[42] The ultrahigh PF of penta-silicene is derived from four hole pockets and relatively flat bands with the same spirit of "pudding-mold" shown in Figure 2c,d.

Lattice Thermal Conductivity. Maybe the lattice thermal conductivity κ_L is the only parameter that can be tuned independently. The calculated phonon transport property of penta-silicene is shown in Figure 4. The phonon dispersion in Figure 4a is free from imaginary numbers, indicating a strong dynamical stability of penta-silicene. The sound velocity is defined as $\upsilon = \left.\frac{\partial\omega}{\partial q}\right|_{q=0}$. The calculated υ of acoustic phonon modes TA and LA are shown in Table 3 (ZA mode is a quadratic function of the wave vector). More details about this parabolic ZA mode can be found in the Supporting Information. υ_{TA} are 3.99 and 4.70 km/s along the *x*- and *y*-axes, respectively. υ_{LA} is larger than υ_{TA}, having values of 4.77 and 5.54 km/s along the *x*- and *y*-axes, respectively. κ_L as a function of temperature is shown in Figure 4b. At room temperature, κ_L of penta-silicene are 1.66 and 1.29 W/mK along *x*- and *y*-axes, respectively. There are two types of scatterings of phonon transport. One is the Normal process and the other one is the Umklapp (U) process. The latter is the only contributor to the final thermal resistance. The touchstone to explore the role of the U process is to study κ_L as a function of temperature. If $\kappa_L \propto \frac{1}{T}$, the U process dominates the heat transport in this material. Figure 4b of penta-silicene shows a good example of this type in heat transport behavior.

According to the Slack model, a small Θ_D generally means a small κ_L since acoustic phonons are the main carrier in heat transport. The definition is $\Theta_D = h\omega_{max}/k_B$ in which ω_{max} is the maximum frequency of the acoustic phonon branches. The calculated Θ_D of penta-silicene is shown in Table 3. The largest Θ_{LA} has a value of 131.51 K along the *x*-axis. This value is about one-fifth that of penta-graphene (Θ_{LA} = 692 K).[56] What is more, the frequency-resolved κ_L of penta-silicene further confirms this discussion. Phonon vibrations below 50 cm^{-1} contribute most to the final κ_L and heat transport whether it is the *x*-axis or the *y*-axis. Phonon relaxation time in Figure 4d also verifies this fact. In the three branches of acoustic phonons, the LA branch has the largest phonon relaxation time compared with the ZA and TA modes. The ultralow κ_L of penta-silicene originates from the weak phonon harmonic interaction and strong anharmonic scattering.[19,57,58] We hope that this low κ_L would induce a high figure of merit ZT of penta-silicene.

Figure of Merit ZT. Based on the above results of electronic and phonon transport properties, one can evaluate the figure of merit ZT written as

$$ZT = \frac{S^2\sigma}{\kappa_e + \kappa_L}T \quad (8)$$

The calculated ZT of penta-silicene for both p-type and n-type are shown in Figure 5. Interestingly, due to the high PF and low κ_L, penta-silicene shows a large ZT (>2) at room temperature for both *x*- and *y*-axes. Specifically, maximum ZT_h (for the hole) has values of 3.43 and 2.24 at 3.42 × 10^{12} and 4.60 × 10^{12} cm^{-2} concentrations along *x*- and *y*-axes at room temperature, respectively. Similarly, maximum ZT_e (for the electron) has values of 2.18 and 3.04 at 2.51 × 10^{12} and 1.85 × 10^{12} cm^{-2} along *x*-and *y*-axes at 300 K. In a graphene-based field-effect transistor, a doping level up to 4 × 10^{14} cm^{-2} for both electrons and holes has been reached by electrical gating[59] and ionic liquid injection.[60] Due to the portability of the experimental technique, 2D materials, like graphene, MoS_2, and black phosphorus, generally can reach 4 × 10^{14} cm^{-2} for both electron and hole doping level. Note that our carrier concentrations (<4 × 10^{14} cm^{-2}) all are reachable in these current experimental technique. Therefore, our result indicates that monolayer penta-silicene is a promising thermoelectric material.

https://dx.doi.org/10.1021/acsami.9b21076
ACS Appl. Mater. Interfaces 2020, 12, 14298−14307

CONCLUSIONS AND DISCUSSION

According to eq 8, the figure of merit ZT is closely related to the temperature. Generally, ZT increases when temperature increases, such as SnSe with a ZT of 2.6 ± 0.3 at 923 K[55] and PbTe−PbS pseudo-binary with a ZT of 2.3 at 923 K.[61] Taking into account the application in daily life, near-room-temperature thermoelectric materials with high ZT are desirable. There is no doubt that Bi_2Te_3-based thermoelectric materials still dominate around room temperature. However, the tellurium element has very low reserves on earth and much expensive. How to find inexpensive thermoelectric material that works efficiently at room temperature is still an open question.[1−3] Very recently, some researchers have made progress in this direction. For example, Mg_3Bi_2 alloy has a ZT of 0.9 at 350 K.[62] Penta-silicene with a ZT of 3.43 probably enriches the room-temperature thermoelectric materials. Besides, how to manipulate defects, lattice symmetry, spin, and electron−phonon coupling to further enhance room-temperature ZT is one of the cutting edges in the thermoelectric field.

For 2D materials, stability is the most important before property. As a matter of fact, metastable phases are quite common in condensed matter. Materials science overwhelmingly deals with metastable states. Besides penta-silicene, many simple light-element compounds including most hydrocarbons, nitrogen oxides, hydrides, carbides, carbon monoxide (CO), alcohols, and glycerin are also metastable at ambient conditions. Nevertheless, the ubiquitous metastable phases do not produce a bad effect on their vast and tremendous applications in modern industrial societies and our daily life. The world has been varied and diverse due to the fact that the metastable states provide the complexity of structures and energy transformation. Furthermore, previous works have successfully obtained penta-silicene nanoribbon on Ag(110) with exotic electronic properties.[4−6,21] At the energy level, the cohesive energy E_c of penta-silicene is 3.92 eV/atom that is comparable with the 3.71 eV/atom[32,33] of silicene (hexagonal symmetry with two atoms in the primitive cell) and 3.61 eV/atom[34,35] of black phosphorene. Note that above two metastable 2D materials, at present, can be easily obtained in experiment based on the advanced experimental technique such as creating a complex chemical environment and variable substrate effect. Besides, we also calculate other two allotropes of penta-silicene. There are Si-*Cmma* and Si-*Pmma*.[38] The calculated E_c of Si-*Cmma* and Si-*Pmma* are 4.17 and 4.18 eV/atom, relatively more stable than penta-silicene.

Moreover, we offer three very promising experimental approaches to make freestanding penta-silicene potentially. Besides, these methods also have great potential for other 2D materials. "Geometrical frustration" was first raised by Joel Therrien who are synthesizing the penta-graphene and other freestanding carbon rings, such as the U-carbon.[63] As far as we can see, penta-silicene has no counterpart in the corresponding bulk material. This fact is quite different from graphene and graphite. Crystalline oxide perovskites, like penta-silicene, also cannot be obtained by mechanical exfoliation. However, monolayer freestanding crystalline oxide perovskites have been grown by "reactive molecular beam epitaxy".[64] Besides, freestanding monolayer amorphous carbon has successfully been created by the "laser-assisted chemical vapor deposition" method.[65] This monolayer amorphous carbon contains five-, six-, seven-, and eight-membered carbon rings. Note that penta-silicene only consists of five-membered silicon rings. Encouraged by these above advanced technologies in the experimental cutting edge, we conclude that monolayer freestanding penta-silicene and other novel nanostructures can also be obtained on the near horizon.

Sometimes, the figure of merit ZT based on the mobility μ in eq 7 is a little overestimated since acoustic phonon is not the only factor to impact the μ that determines the final ZT. As we mentioned before, nonpolar optical phonons and ionized impurities also influence μ. Generally, the impact of these two factors can be neglected and the role of longitudinal acoustic phonons is dominant.[12,51,66,67] Given that realistic calculation of couplings between nonpolar optical phonons and electrons, ionized impurities and electrons are beyond our current computing capabilities, and they are interesting open questions that deserve further exploration.

The DP theory is based on the rigid band approximation. Surprisingly, this approximation works well for most cases when the electronic bands around the Fermi level are not highly degenerate.[42,68] Besides, VASP, Quantum ESPRESSO, and BoltzTraP softwares,[27−30] to name a few, also can add electrons into or remove electrons from the system through a compensating uniform charge background of opposite sign to maintain charge neutrality, which verifies the correctness of this approximation additionally.

The DP theory has been widely used and has been successful in calculating the intrinsic (freestanding and defect-free) mobility, which can be found everywhere. Certainly, almost any theoretical model has assumptions, either large or small, such as the famous density functional theory, Dulong−Petit law (high temperature), and even Newton's laws of motion (inertial system). The DP theory is also included. As a matter of fact, in the DP theory, only the longitudinal-acoustic phonon is considered without any dispersion and the electron−phonon matrix is expressed by the DP constant and the elastic constant that are described in the eq 7. The optical phonon scatterings are absent in the DP theory. However, DP theory's results are qualitatively and even quantitatively reasonable in many cases compared with the full evaluation of electron−phonon coupling.[69] Since this calculation is far beyond our current computational capabilities, hence, we suggest leaving the e−ph coupling as an open question, which should be explored further.

How a 2D functional material, like our penta-silicene, is to be used in bulk devices? There are four options to integrate bulk materials with 2D materials for physical coupling and applications.[70] On the one hand, one can construct 2D materials on 3D materials (2D-on-3D) heterostructures. The technique methods are van der Waals epitaxy (vdWE), wet transfer, and the metal-induced quasi-dry transfer process. On the other hand, the realization of 3D-to-2D heterostructures is still at a premature stage. However, the relevant experiment is growing fast, which has significantly broadened the material beyond conventional 3D material-based heterostructures.

In summary, we have calculated the thermoelectric performance of monolayer penta-silicene by first-principles. It has good thermal, dynamical, and mechanical stability compared with many other typical 2D materials, such as hexagonal silicene and black phosphorous. Lattice thermal conductivities of penta-silicene have values of 1.66 and 1.29 W/mK along *x*- and *y*-axes, respectively. Superior electronic properties originate from the "pudding-mold-like" shape of valence bands around the Fermi level. Ultralow thermal conductivity and high power

https://dx.doi.org/10.1021/acsami.9b21076
ACS Appl. Mater. Interfaces 2020, 12, 14298−14307

factor collaboratively lead to an ultrahigh ZT of penta-silicene. At room temperature, maximum ZT has values of 3.43 and 3.04 for hole doping and electron doping, respectively. Our work has indicated that penta-silicene is a promising thermoelectric material, especially at near room temperature. The layer-dependent thermoelectric property of penta-silicene deserves more follow up study in the future.

■ ASSOCIATED CONTENT

Supporting Information

The Supporting Information is available free of charge at https://pubs.acs.org/doi/10.1021/acsami.9b21076.

Room-temperature lattice thermal conductivity of penta-silicene as a function of the cutoff for the interaction range of anharmonic force constants and phonon dispersion superposed on the spectra from the continuum theory (PDF)

■ AUTHOR INFORMATION

Corresponding Author

Zhibin Gao − *Department of Physics, National University of Singapore, Singapore 117551, Republic of Singapore;* orcid.org/0000-0002-6843-381X; Email: zhibin.gao@nus.edu.sg

Author

Jian-Sheng Wang − *Department of Physics, National University of Singapore, Singapore 117551, Republic of Singapore*

Complete contact information is available at: https://pubs.acs.org/10.1021/acsami.9b21076

Notes

The authors declare no competing financial interest.

■ ACKNOWLEDGMENTS

The authors are grateful to Wu Li for the kind guidance on calculation of lattice thermal conductivity. We acknowledge Jinyang Xi for many fruitful discussions and good suggestions. We also thank Wen Shi and Tianqi Deng for valuable discussions and kind help. We acknowledge the financial support from MOE tier 1 funding of NUS Faculty of Science, Singapore (grant no. R-144-000-402-114).

■ REFERENCES

(1) Goodilin, E. A.; Weiss, P. S.; Gogotsi, Y. Nanotechnology Facets of the Periodic Table of Elements. *ACS Nano* **2019**, *13*, 10879−10886.

(2) Tao, L.; Cinquanta, E.; Chiappe, D.; Grazianetti, C.; Fanciulli, M.; Dubey, M.; Molle, A.; Akinwande, D. Silicene FieldEffect Transistors Operating at Room Temperature. *Nat. Nanotechnol.* **2015**, *10*, 227.

(3) Tsai, W.-F.; Huang, C.-Y.; Chang, T.-R.; Lin, H.; Jeng, H.-T.; Bansil, A. Gated Silicene as a Tunable Source of Nearly 100% Spin-Polarized Electrons. *Nat. Commun.* **2013**, *4*, 1500.

(4) Cerdá, J. I.; Sławińska, J.; Le Lay, G.; Marele, A. C.; Gómez-Rodríguez, J. M.; Dávila, M. E. Unveiling the Pentagonal Nature of Perfectly Aligned Singleand Double-Strand Si Nano-Ribbons on Ag(110). *Nat. Commun.* **2016**, *7*, 13076.

(5) Prévot, G.; Hogan, C.; Leoni, T.; Bernard, R.; Moyen, E.; Masson, L. Si Nanoribbons on Ag(110) Studied by Grazing-Incidence X-Ray Diffraction, Scanning Tunneling Microscopy, and Density-Functional Theory: Evidence of a Pentamer Chain Structure. *Phys. Rev. Lett.* **2016**, *117*, 276102.

(6) Sheng, S.; Ma, R.; Wu, J. B.; Li, W.; Kong, L.; Cong, X.; Cao, D.; Hu, W.; Gou, J.; Luo, J.-W.; Cheng, P.; Tan, P.-H.; Jiang, Y.; Chen, L.; Wu, K. The Pentagonal Nature of Self-Assembled Silicon Chains and Magic Clusters on Ag (110). *Nano Lett.* **2018**, *18*, 2937−2942.

(7) He, J.; Tritt, T. M. Advances in Thermoelectric Materials Research: Looking Back and Moving Forward. *Science* **2017**, *357*, eaak9997.

(8) Snyder, G. J.; Toberer, E. S. Complex Thermoelectric Materials. *Nat. Mater.* **2008**, *7*, 105−114.

(9) Lee, S.; Esfarjani, K.; Luo, T.; Zhou, J.; Tian, Z.; Chen, G. Resonant Bonding Leads to Low Lattice Thermal Conductivity. *Nat. Commun.* **2014**, *5*, 3525.

(10) Nielsen, M. D.; Ozolins, V.; Heremans, J. P. Lone Pair Electrons Minimize Lattice Thermal Conductivity. *Energy Environ. Sci.* **2013**, *6*, 570−578.

(11) Heremans, J. P.; Jovovic, V.; Toberer, E. S.; Saramat, A.; Kurosaki, K.; Charoenphakdee, A.; Yamanaka, S.; Snyder, G. J. Enhancement of Thermoelectric Efficiency in PbTe by Distortion of the Electronic Density of States. *Science* **2008**, *321*, 554−557.

(12) Pei, Y.; Shi, X.; LaLonde, A.; Wang, H.; Chen, L.; Snyder, G. J. Convergence of Electronic Bands for High Performance Bulk Thermoelectrics. *Nature* **2011**, *473*, 66.

(13) Liu, W.; Tan, X.; Yin, K.; Liu, H.; Tang, X.; Shi, J.; Zhang, Q.; Uher, C. Convergence of Conduction Bands as a Means of Enhancing Thermoelectric Performance of n-Type $Mg_2Si_{1-x}Sn_x$ Solid Solutions. *Phys. Rev. Lett.* **2012**, *108*, 166601.

(14) Dresselhaus, M. S.; Chen, G.; Tang, M. Y.; Yang, R. G.; Lee, H.; Wang, D. Z.; Ren, Z. F.; Fleurial, J.-P.; Gogna, P. New Directions for Low-Dimensional Thermoelectric Materials. *Adv. Mater.* **2007**, *19*, 1043−1053.

(15) Zhang, S.; Zhou, J.; Wang, Q.; Chen, X.; Kawazoe, Y.; Jena, P. Penta-Graphene: A New Carbon Allotrope. *Proc. Natl. Acad. Sci. U. S. A.* **2015**, *112*, 2372−2377.

(16) Ressouche, E.; Simonet, V.; Canals, B.; Gospodinov, M.; Skumryev, V. Magnetic Frustration in an Iron-Based Cairo Pentagonal Lattice. *Phys. Rev. Lett.* **2009**, *103*, 267204.

(17) Wu, X.; Varshney, V.; Lee, J.; Zhang, T.; Wohlwend, J. L.; Roy, A. K.; Luo, T. Hydrogenation of Penta-Graphene Leads to Unexpected Large Improvement in Thermal Conductivity. *Nano Lett.* **2016**, *16*, 3925−3935.

(18) Liu, H.; Qin, G.; Lin, Y.; Hu, M. Disparate Strain Dependent Thermal Conductivity of Two-Dimensional PentaStructures. *Nano Lett.* **2016**, *16*, 3831−3842.

(19) Gao, Z.; Zhang, Z.; Liu, G.; Wang, J.-S. Ultralow Lattice Thermal Conductivity of Monolayer Penta-Silicene and PentaGermanene. *Phys. Chem. Chem. Phys.* **2019**, 26033−26040.

(20) Oyedele, A. D.; Yang, S.; Feng, T.; Haglund, A. V.; Gu, Y.; Puretzky, A. A.; Briggs, D.; Rouleau, C. M.; Chisholm, M. F.; Unocic, R. R.; Mandrus, D.; Meyer, H. M., III; Pantelides, S. T.; Geohegan, D. B.; Xiao, K. Defect-Dediated Phase Transformation in Anisotropic Two-D $PdSe_2$ Crystals for Seamless Electrical Contacts. *J. Am. Chem. Soc.* **2019**, *141*, 8928−8936.

(21) Guo, Y.; Zhang, C.; Zhou, J.; Wang, Q.; Jena, P. Lattice Dynamic and Instability in Pentasilicene: A Light Single-Element Ferroelectric Material With High Curie Temperature. *Phys. Rev. Appl.* **2019**, *11*, No. 064063.

(22) Blöchl, P. E. Projector Augmented-Wave Method. *Phys. Rev. B: Condens. Matter Mater. Phys.* **1994**, *50*, 17953−17979.

(23) Kresse, G.; Joubert, D. From Ultrasoft Pseudopotentials to the Projector Augmented-Wave Method. *Phys. Rev. B: Condens. Matter Mater. Phys.* **1999**, *59*, 1758−1775.

(24) Perdew, J. P.; Burke, K.; Ernzerhof, M. Generalized Gradient Approximation Made Simple. *Phys. Rev. Lett.* **1996**, *77*, 3865−3868.

(25) Heyd, J.; Scuseria, G. E.; Ernzerhof, M. Hybrid Functionals Based on a Screened Coulomb Potential. *J. Chem. Phys.* **2003**, *118*, 8207−8215.

(26) Krukau, A. V.; Vydrov, O. A.; Izmaylov, A. F.; Scuseria, G. E. Influence of the Exchange Screening Parameter on the Performance of Screened Hybrid Functionals. *J. Chem. Phys.* **2006**, *125*, 224106.

(27) Kresse, G.; Furthmüller, J. Efficient Iterative Schemes for Ab Initio Total-Energy Calculations Using A Plane-Wave Basis Set. *Phys. Rev. B* **1996**, *54*, 11169−11186.
(28) Kresse, G.; Furthmüller, J. Efficiency of Ab-Initio Total Energy Calculations for Metals and Semiconductors Using A Plane-Wave Basis Set. *Comput. Mater. Sci.* **1996**, *6*, 15−50.
(29) Kresse, G.; Hafner, J. Ab Initio MolecularDynamics Simulation of the LiquidMetal−Amorphous-Semiconductor Transition in Germanium. *Phys. Rev. B: Condens. Matter Mater. Phys.* **1994**, *49*, 14251−14269.
(30) Madsen, G. K. H.; Singh, D. J. BoltzTraP. A Code for Calculating Band-Structure Dependent Quantities. *Comput. Phys. Commun.* **2006**, *175*, 67−71.
(31) Li, W.; Carrete, J.; Katcho, N. A.; Mingo, N. ShengBTE: A Solver of the Boltzmann Transport Equation for Phonons. *Comput. Phys. Commun.* **2014**, *185*, 1747.
(32) Fleurence, A.; Friedlein, R.; Ozaki, T.; Kawai, H.; Wang, Y.; Yamada-Takamura, Y. Experimental Evidence for Epitaxial Silicene on Diboride Thin Films. *Phys. Rev. Lett.* **2012**, *108*, 245501.
(33) Feng, B.; Ding, Z.; Meng, S.; Yao, Y.; He, X.; Cheng, P.; Chen, L.; Wu, K. Evidence of Silicene in Honeycomb Structures of Silicon on Ag (111). *Nano Lett.* **2012**, *12*, 3507−3511.
(34) Liu, H.; Neal, A.; Zhu, Z.; Luo, Z.; Xu, X.; Tománek, D.; Ye, P. D. Phosphorene: An Unexplored 2D Semiconductor with A High Hole Mobility. *ACS Nano* **2014**, *8*, 4033−4041.
(35) Li, L.; Yu, Y.; Ye, G. J.; Ge, Q.; Ou, X.; Wu, H.; Feng, D.; Chen, X. H.; Zhang, Y. Black Phosphorus Field-Effect Transistors. *Nat. Nanotechnol.* **2014**, *9*, 372.
(36) Liu, D.; Every, A. G.; Tománek, D. Continuum Approach for Long-Wavelength Acoustic Phonons in Quasi-TwoDimensional Structures. *Phys. Rev. B: Condens. Matter Mater. Phys.* **2016**, *94*, 165432.
(37) Gao, Z.; Dong, X.; Li, N.; Ren, J. Novel Two-Dimensional Silicon Dioxide with In-Plane Negative Poisson's Ratio. *Nano Lett.* **2017**, *17*, 772−777.
(38) Zhou, N.; Zhou, P.; Li, J.; He, C.; Zhong, J. Si-Cmma: A Silicon Thin Film with Excellent Stability and Dirac Nodal Loop. *Phys. Rev. B: Condens. Matter Mater. Phys.* **2019**, *100*, 115425.
(39) Gao, Z.; Liu, D.; Tománek, D. TwoDimensional Mechanical Metamaterials with Unusual Poisson Ratio Behavior. *Phys. Rev. Appl.* **2018**, *10*, No. 064039.
(40) Zhu, Z.; Cai, X.; Yi, S.; Chen, J.; Dai, Y.; Niu, C.; Guo, Z.; Xie, M.; Liu, F.; Cho, J.-H.; Jia, Y.; Zhang, Z. Multivalency-Driven Formation of Te-Based Monolayer Materials: A Combined First-Principles and Experimental study. *Phys. Rev. Lett.* **2017**, *119*, 106101.
(41) Guo, R.; Wang, X.; Kuang, Y.; Huang, B. First-Principles Study of Anisotropic Thermoelectric Transport Properties of IV-VI Semiconductor Compounds SnSe and SnS. *Phys. Rev. B: Condens. Matter Mater. Phys.* **2015**, *92*, 115202.
(42) Gao, Z.; Liu, G.; Ren, J. High Thermoelectric Performance in Two-Dimensional Tellurium: An Ab Initio Study. *ACS Appl. Mater. Interfaces* **2018**, *10*, 40702−40709.
(43) Li, M.; Wang, N.; Jiang, M.; Xiao, H.; Zhang, H.; Liu, Z.; Zu, X.; Qiao, L. Improved Thermoelectric Performance of Bilayer Bi2O2Se by the Band Convergence Approach. *J. Mater. Chem. C* **2019**, *7*, 11029−11039.
(44) Toberer, E. S.; Baranowski, L. L.; Dames, C. Advances in Thermal Conductivity. *Annu. Rev. Mater. Res.* **2012**, *42*, 179−209.
(45) Wang, F. Q.; Guo, Y.; Wang, Q.; Kawazoe, Y.; Jena, P. Exceptional Thermoelectric Properties of Layered GeAs2. *Chem. Mater.* **2017**, *29*, 9300−9307.
(46) Bahk, J.-H.; Shakouri, A. Minority Carrier Blocking to Enhance the Thermoelectric Figure of Merit in Narrow-Band-Gap Semiconductors. *Phys. Rev. B: Condens. Matter Mater. Phys.* **2016**, *93*, 165209.
(47) Chang, C.; Wu, M.; He, D.; Pei, Y.; Wu, C.-F.; Wu, X.; Yu, H.; Zhu, F.; Wang, K.; Chen, Y.; Huang, L.; Li, J.-F.; He, J.; Zhao, L.-D. 3D Charge and 2D Phonon Transports Leading to High Out-of-Plane ZT in n-Type SnSe Crystals. *Science* **2018**, *360*, 778−783.
(48) Bilc, D. I.; Hautier, G.; Waroquiers, D.; Rignanese, G.-M.; Ghosez, P. LowDimensional Transport and Large Thermoelectric Power Factors in Bulk Semiconductors by Band Engineering of Highly Directional Electronic States. *Phys. Rev. Lett.* **2015**, *114*, 136601.
(49) He, J.; Amsler, M.; Xia, Y.; Naghavi, S. S.; Hegde, V. I.; Hao, S.; Goedecker, S.; Ozoliņš, V.; Wolverton, C. Ultralow Thermal Conductivity in Full Heusler Semiconductors. *Phys. Rev. Lett.* **2016**, *117*, No. 046602.
(50) Popescu, A.; Woods, L. M.; Martin, J.; Nolas, G. S. Model of Transport Properties of Thermoelectric Nanocomposite Materials. *Phys. Rev. B: Condens. Matter Mater. Phys.* **2009**, *79*, 205302.
(51) Qiao, J.; Kong, X.; Hu, Z.-X.; Yang, F.; Ji, W. High-Mobility Transport Anisotropy and Linear Dichroism in Few-Layer Black Phosphorus. *Nat. Commun.* **2014**, *5*, 4475.
(52) Mahan, G. D.; Sofo, J. O. The Best Thermoelectric. *Proc. Natl. Acad. Sci. U. S. A.* **1996**, *93*, 7436−7439.
(53) Kuroki, K.; Arita, R. "Pudding Mold" Band Drives Large Thermopower in Na_xCoO_2. *J. Phys. Soc. Jpn.* **2007**, *76*, No. 083707.
(54) Usui, H.; Suzuki, K.; Kuroki, K.; Nakano, S.; Kudo, K.; Nohara, M. Large Seebeck Effect in Electron-Doped FeAs2 Driven by a Quasi-One-Dimensional Pudding-Mold-Type Band. *Phys. Rev. B: Condens. Matter Mater. Phys.* **2013**, *88*, No. 075140.
(55) Zhao, L.-D.; Lo, S.-H.; Zhang, Y.; Sun, H.; Tan, G.; Uher, C.; Wolverton, C.; Dravid, V. P.; Kanatzidis, M. G. Ultralow Thermal Conductivity and High Thermoelectric Figure of Merit in SnSe Crystals. *Nature* **2014**, *508*, 373−377.
(56) Wang, F. Q.; Yu, J.; Wang, Q.; Kawazoe, Y.; Jena, P. Lattice Thermal Conductivity of Penta-Graphene. *Carbon* **2016**, *105*, 424−429.
(57) Bao, H.; Chen, J.; Gu, X.; Cao, B. A Review of Simulation Methods in Micro/Nanoscale Heat Conduction. *ES Energy Environ.* **2018**, *1*, 16−55.
(58) Ouyang, T.; Jiang, E.; Tang, C.; Li, J.; He, C.; Zhong, J. Thermal and Thermoelectric Properties of Monolayer Indium Triphosphide (InP3): A First-Principles Study. *J. Mater. Chem. A* **2018**, *6*, 21532−21541.
(59) Efetov, D. K.; Kim, P. Controlling Electron-Phonon Interactions in Graphene at Ultrahigh Carrier Densities. *Phys. Rev. Lett.* **2010**, *105*, 256805.
(60) Chuang, H.-J.; Tan, X.; Ghimire, N. J.; Perera, M. M.; Chamlagain, B.; Cheng, M. M.-C.; Yan, J.; Mandrus, D.; Tománek, D.; Zhou, Z. High Mobility WSe2 p-and n-Type Field-Effect Transistors Contacted by Highly Doped Graphene for Low-Resistance Contacts. *Nano Lett.* **2014**, *14*, 3594−3601.
(61) Wu, D.; Zhao, L.-D.; Tong, X.; Li, W.; Wu, L.; Tan, Q.; Pei, Y.; Huang, L.; Li, J.-F.; Zhu, Y.; Kanatzidis, M. G.; He, J. Superior Thermoelectric Performance in PbTe−PbS Pseudo-Binary: Extremely Low Thermal Conductivity and Modulated Carrier Concentration. *Energy Environ. Sci.* **2015**, *8*, 2056−2068.
(62) Mao, J.; Zhu, H.; Ding, Z.; Liu, Z.; Gamage, G. A.; Chen, G.; Ren, Z. High Thermoelectric Cooling Performance of n-Type Mg3Bi2-Based Materials. *Science* **2019**, *365*, 495−498.
(63) Gibbs, W. W. A New Form of Pure Carbon Dazzles and Attracts. *Science* **2019**, *366*, 782−783.
(64) Ji, D.; Cai, S.; Paudel, T. R.; Sun, H.; Zhang, C.; Han, L.; Wei, Y.; Zang, Y.; Gu, M.; Zhang, Y.; Gao, W.; Huyan, H.; Guo, W.; Wu, D.; Gu, Z.; Tsymbal, E. Y.; Wang, P.; Nie, Y.; Pan, X. Freestanding Crystalline Oxide Perovskites Down To the Monolayer Limit. *Nature* **2019**, *570*, 87.
(65) Toh, C.-T.; Zhang, H.; Lin, J.; Mayorov, A. S.; Wang, Y.-P.; Orofeo, C. M.; Ferry, D. B.; Andersen, H.; Kakenov, N.; Guo, Z.; Abidi, I. H.; Sims, H.; Suenaga, K.; Pantelides, S. T.; Özyilmaz, B. Synthesis and Properties of Free-Standing Monolayer Amorphous Carbon. *Nature* **2020**, *577*, 199−203.
(66) Bardeen, J.; Shockley, W. Deformation Potentials and Mobilities in Non-Polar Crystals. *Phys. Rev.* **1950**, *80*, 72−80.
(67) Wang, H.; Pei, Y.; LaLonde, A. D.; Snyder, G. J. Weak Electron−Phonon Coupling Contributing to High Thermoelectric

https://dx.doi.org/10.1021/acsami.9b21076
ACS Appl. Mater. Interfaces 2020, 12, 14298−14307

Performance in N-Type PbSe. *Proc. Natl. Acad. Sci. U. S. A.* **2012**, *109*, 9705−9709.
(68) Gao, Z.; Zhou, Z.; Tománek, D. Degenerately Doped Transition Metal Dichalcogenides as Ohmic Homojunction Contacts to Transition Metal Dichalcogenide Semiconductors. *ACS Nano* **2019**, *13*, 5103−5111.
(69) Nakamura, Y.; Zhao, T.; Xi, J.; Shi, W.; Wang, D.; Shuai, Z. Intrinsic Charge Transport in Stanene: Roles of Bucklings and Electron−Phonon Couplings. *Adv. Electron. Mater.* **2017**, *3*, 1700143.
(70) Bae, S.-H.; Kum, H.; Kong, W.; Kim, Y.; Choi, C.; Lee, B.; Lin, P.; Park, Y.; Kim, J. Integration of bulk materials with two-dimensional materials for physical coupling and applications. *Nat. Mater.* **2019**, *18*, 550−560.

https://dx.doi.org/10.1021/acsami.9b21076
ACS Appl. Mater. Interfaces 2020, 12, 14298−14307